Ecotoxicology and Environmental Safety 253 (2023) 114647

Contents lists available at ScienceDirect

Ecotoxicology and Environmental Safety

journal homepage: www.elsevier.com/locate/ecoenv

Co-exposure to arsenic and fluoride to explore the interactive effect on oxidative stress and autophagy in myocardial tissue and cell

Xiaolin Tian [a,c], Meng Wang [a], Xiaodong Ying [a], Nisha Dong [b], Meng Li [a], Jing Feng [d], Yannan Zhao [a], Qian Zhao [a], Fengjie Tian [a], Ben Li [a], Wenping Zhang [a], Yulan Qiu [a], Xiaoyan Yan [a,*]

[a] School of Public Health, Shanxi Medical University, Taiyuan, Shanxi 030001, China
[b] Heping Hospital Affiliated To Changzhi Medical College, Changzhi, Shanxi 046000, China
[c] School of Public Health, Zhejiang Chinese Medical University, Hangzhou, Zhejiang 310053, China
[d] Laboratory of Cardiovascular Medicine, The Second Hospital of Shanxi Medical University, Taiyuan, Shanxi 030001, China

ARTICLE INFO

Edited by Dr Yong Liang

Keywords:
Arsenic
Fluoride
Interaction
Cardiotoxicity

ABSTRACT

Co-contamination of arsenic and fluoride is widely distributed in groundwater. However, little is known about the interactively influence of arsenic and fluoride, especially the combined mechanism in cardiotoxicity. Cellular and animal models exposure to arsenic and fluoride were established to assess the oxidative stress and autophagy mechanism of cardiotoxic damage using the factorial design, a widely used statistical method for assessing two factor interventions. In vivo, combined exposure to high arsenic (50 mg/L) and high fluoride (100 mg/L) induced myocardial injury. The damage is accompanied by accumulation of myocardial enzyme, mitochondrial disorder, and excessive oxidative stress. Further experiment identified that arsenic and fluoride induced the accumulation of autophagosome and increased expression level of autophagy related genes during the cardiotoxicity process. These findings were further demonstrated through the in vitro model of arsenic and fluoride-treated the H9c2 cells. Additionally, combined of arsenic-fluoride exposure possesses the interactively influence on oxidative stress and autophagy, contributing to the myocardial cell toxicity. In conclusion, our data suggest that oxidative stress and autophagy are involved in the process of cardiotoxic injury, and that these indicators showed interaction effect in response to the combined exposure of arsenic and fluoride.

1. Introduction

As the 20th and the 13th most abundant elements in the earth crust, arsenic and fluorine are widely distributed in the ground fresh water around the globe (Rocha-Amador et al., 2007; Wang et al., 2007a). The dominant reason of the excessive accumulation for arsenic and fluoride in groundwater is natural and human factors, such as natural sedimentation of minerals and rocks, mining, metal smelting, and the use of pesticides (Mondal and Chattopadhyay, 2020). Cumulative studies have demonstrated that co-contamination of arsenic and fluoride in groundwater is conspicuously distributed in semi-arid areas of many countries, such as China, the United States, Mexico, and Pakistan (Kumar et al., 2020). Of note, from a geochemical point of view, there is an appreciable correlation between arsenic and fluoride, and it is even discovered that the occurrence of arsenic and fluoride complexes in groundwater (Bundschuh et al., 2004; Sivasankar et al., 2016). Therefore, it has been undoubtedly logical and necessary to further clarify the interactively toxic mechanism(s) about arsenic and fluoride.

Though accumulating epidemiological investigations and laboratory data have revealed that individual toxicity of arsenic and fluoride, the cognition of combined toxic mechanism is still insufficient. Notably, the positive correlation between arsenic and fluoride was revealed on the adverse health effects in epidemiological studies of Mexico, therefore, the interactive toxicity related health risks deserve immediate attention (Armienta and Segovia, 2008; González-Horta et al., 2015). Several animal and cell studies further demonstrated that the arsenic and fluoride showed differently combined effect depending on the confounding factors (exposure time, dose and object) (Flora et al., 2011; Mittal et al.,

Abbreviations: As, arsenic; F, fluoride; GSH-Px, glutathione peroxidase; SOD, superoxide dismutase; MDA, malondialdehyde; LDH, lactate dehydrogenase; ROS, reactive oxygen species; TEM, transmission electron microscopy.

* Correspondence to: School of Public Health, Shanxi Medical University, Shanxi 030001, China.
E-mail address: yanxiaoyan@sxmu.edu.cn (X. Yan).

https://doi.org/10.1016/j.ecoenv.2023.114647
Received 24 October 2022; Received in revised form 6 February 2023; Accepted 11 February 2023
Available online 15 February 2023

2018; Rocha et al., 2011; Sárközi et al., 2015). Based on the nephrotoxicity animal models of factorial design and the statistical method of factorial analysis, our previous studies were the first to evaluate the interaction between arsenic and fluoride, and the various indicators of oxidative stress showed the differently combined effect (Tian et al., 2019; Tian et al., 2020). In addition, arsenic and fluoride showed antagonistic effect on inflammation and oxidative stress in primary human umbilical vein endothelial cells (Ma et al., 2017). Moreover, compared to the single arsenic and fluoride exposure, combined exposure also showed the attenuated effect on the RNA and protein levels of inflammatory-related molecules in rabbit aorta (Ma et al., 2012). Therefore, although it is well documented that the interactive toxicity about arsenic and fluoride has an adverse effect on the exposure population and animal, the mechanism of the interactive influence is still unclear and needs to be studied systematically.

The syndrome of endemic arsenism and fluorosis generally shares the same disease characteristics as two single virulence, such as dental and skeletal fluorosis, multiple skin lesions, and other soft tissue injury (Alarcón-Herrera et al., 2020; Chakraborti et al., 2016). Notably, researchers found that high concentrations of arsenic and fluorine may have been the important factor to accelerate cardiovascular disease. Specifically, the high levels of arsenic in drinking water (≥100 μg/l) was the key factor to establish the association between arsenic and clinical CVD endpoints in multiple studies (Moon et al., 2012; Tsuji et al., 2014). More importantly, epidemiological studies in southwestern Taiwan, showed that the high dose (700–930 μg/l) increased the occur of Hypertension, Ischemic heart disease and Carotid atherosclerosis (Huang et al., 2007; Wang et al., 2007b). The high dose of arsenic exposure significantly increased aortic lesions, fatty streak lesions in aortic arch and valves, defective vasorelaxation in ApoE-knockout mice (Simeonova et al., 2003; Srivastava et al., 2007). In addition, we recently published a Systematic Review and Meta-Analysis supported the possibility of a positive correlation between fluoride exposure and blood pressure in endemic fluorosis areas (Li et al., 2021), this finding was confirmed in another study (Li et al., 2021). A Cross-sectional analysis to prove the relationship of high fluoride(>3.01 mg/L) exposure and atherosclerosis. Animal studies also confirm the high dose of 150 mg/l, 300 mg/l and 600 mg/l NaF exposure induced hypertension and cardiovascular complications in male rats (Oyagbemi et al., 2017). More recently, emerging evidence in rabbits and endothelial cells reported that combined of arsenic and fluoride induced vasculotoxic lesion accompanied by oxidative stress and inflammatory; moreover, arsenic and fluoride showed antagonistic effect in this damage process (Ma et al., 2017; Ma et al., 2012). In addition, our recent report showed that co-exposure to arsenic and fluoride altered the cardiac function, including blood pressure, heart rate, electrocardiogram and echocardiogram (Yan et al., 2021). These studies strongly supported that combined exposure of arsenic and fluoride is associated with the cardiovascular disease. However, the underlying interactive mechanism of arsenic and fluoride inducing myocardial injury is still not completely elucidated.

Further systematacially elucidating the molecular mechanism of myocardial injury induced by arsenic and fluoride alone and combined has become an indispensable part to achieve research objectives in current study. It is understood that autophagy is a highly conserved lysosomal catabolism mechanism, in which damaged organelles and macrobiotic proteins are wrapped in autophagosomes and transported to lysosomes for degradation (Gu et al., 2016; Zhuang et al., 2016). As the energy provider for cellular activities, oxidative phosphorylation of mitochondria is accompanied by potential hazards of excessive ROS, while the autophagy has been defined as an important buffer systems in response to oxidative stress or mitochondrial dysfunction (Wang and Klionsky, 2011; Yamashita and Kanki, 2017; Yi et al., 2018). Mounting evidence suggests that the regulation of autophagy has been implicated in cardiovascular disease (Daniels et al., 2019). A previous study revealed that excessive autophagy was linked to dysfunctional mitochondria and cellular homeostasis imbalance in the myocardium and was involved in acute heart failure, myocardial hypertrophy, and other chronic heart disease (Che et al., 2021; Chi et al., 2021; Zhao et al., 2021). However, how combined of arsenic-fluoride exposure disrupts the occurrence of autophagy in cardiomyocytes and whether such aberrant regulation contributes to cardiotoxic injury remain unknown.

Therefore, we aimed to evaluate the interactive influence mechanism of arsenic and fluoride in myocardial tissue and cell. For this research purpose, the 2 × 3 factorial design cell model and 2 × 2 factorial design animal model were established to assess the oxidative stress and autophagy mechanism of cardiotoxic damage. More importantly, confronting with the phenomenon that of co-contamination of arsenic and fluoride in groundwater, we for the first time used the concept of two-factor and multi-level factorial design to specifically explore the interaction between arsenic and fluoride in this study.

2. Materials and methods

2.1. Animals and treatments

Healthy adult Sprague Dawley rats (200–250 g) were provided by the Laboratory Animal Center of Shanxi Medical University, Taiyuan, China (certificate No SYXK 2019–0007, Grade SPF). The rats were kept in barrier environment of Laboratory Animal Center of Shanxi Medical University and maintained at suitable temperature, humidity, and light/dark cycle. The experimental protocol was approved by the Institutional Animal Care and Use Committee of Shanxi Medical University (No. 2019LL002).

The parental male and female rats (for mating at the 1:2 male to female ratio) were randomly divided into four groups: control group, F group (100 mg/L NaF), As group (50 mg/L $NaAsO_2$), and F+As group (100 mg/L NaF and 50 mg/L $NaAsO_2$). Pregnant rats were provided free access to drinking water (NaF and/or $NaAsO_2$) from the first day of pregnancy to the 21st day after giving birth. Rat pups were exposed to arsenic and/or fluoride through their mothers during gestation and lactation, then through drinking the same treatment water as their mothers until postnatal day 90 (Fig. 1A). The dosages of fluoride and arsenic were chosen based on previous studies in rat offspring (Tian et al., 2020; Yan et al., 2021). The three-month-old male rat pups were sacrificed, and the hearts of offspring rats were isolated and weighted. Three myocardial tissues of each group were fixed in paraformaldehyde and glutaraldehyde for morphological observation. The other myocardial tissues were frozen immediately with liquid nitrogen and preserved at − 80 ℃ for subsequent experiments. Each animal experiment data represented the averages of 5 independent experiments.

2.2. Biochemical analysis

Myocardial tissue was broken up to fully release the protease using SCIENTZ - IID ultrasonic crusher (Ningbo Xinzhi organism co., LTD, China). The conditions were as follows: 80 Hz, 5 s for each ultrasound, 10 s pause, 2 min, 8 times in total. The subsequent procedures were carried out according to the instructions of glutathione peroxidase (GSH-Px), superoxide dismutase (SOD), malondialdehyde (MDA), lactate dehydrogenase (LDH) and Na^+/K^+-ATPase kit (Nanjing jiancheng bioengineering institute, China), and the results were determined by the automatic microplate reader (BioTek, USA).

2.3. Observation of optical microscopy

For myocardial tissue, the extent of myocardial injury was assessed by histopathological analysis. The fresh hearts were fixed, dried, paraffined and embedded in paraffin, then they were sliced to paraffin-embedded sections (at 4 μm thickness). Then the sections were spread, dried, dewaxed, and stained by Hematoxylin and Eosin (HE) Staining Kit (Beyotime Institute of Biotechnology, China). Finally, the stained sections of myocardial tissue were observed using the Olympus optical

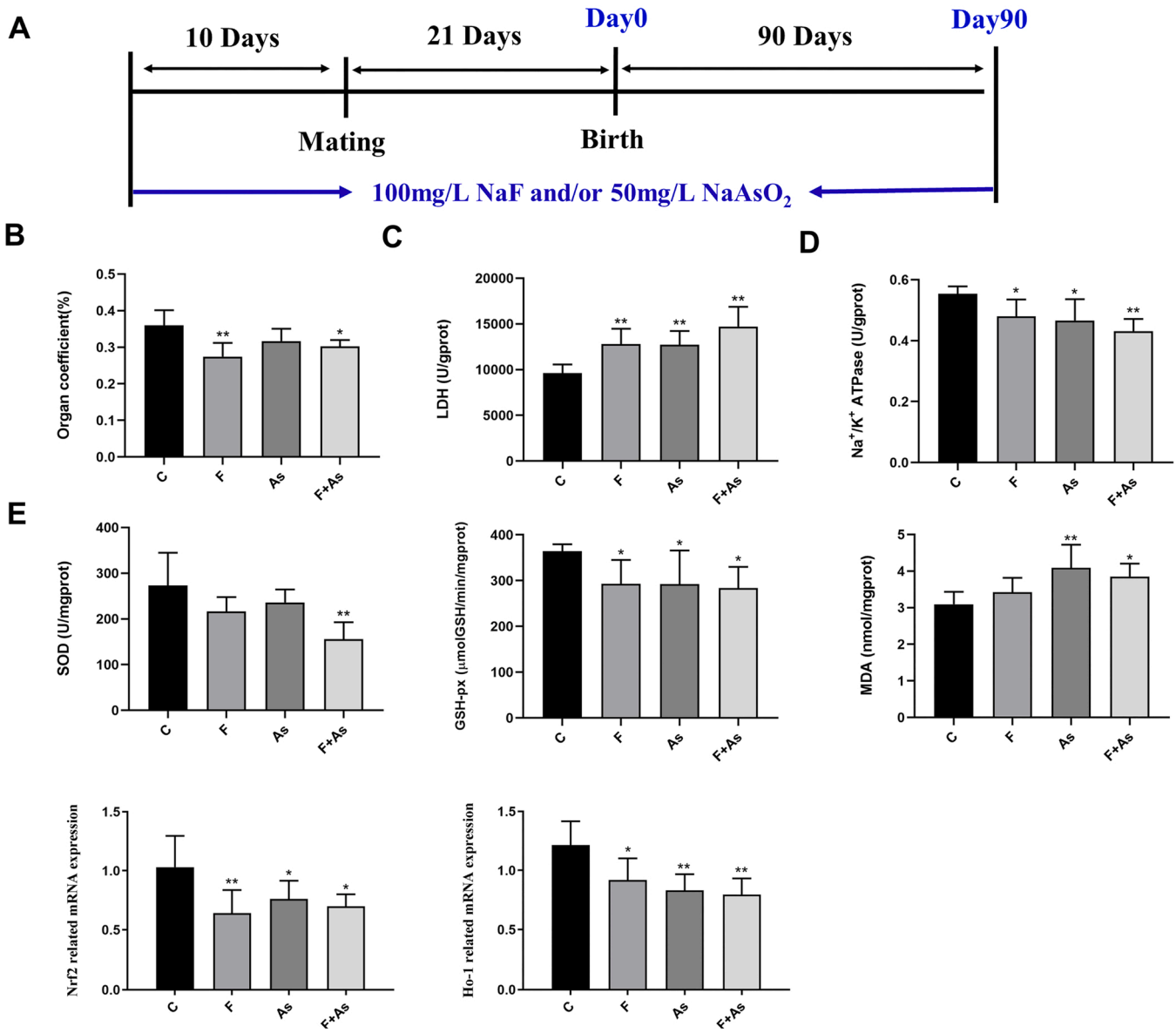

Fig. 1. Arsenic and fluoride exposure induced myocardial injury and oxidative stress in offspring rat. (A) Scheme of fluoride and arsenic exposure. (B) Organ coefficient of the heart. (C-D) Enzyme activity of LDH and Na^+/K^+ ATPase in myocardial tissue. (E) Oxidative stress related indicators in myocardial tissue, including SOD, GSH-PX, MDA, Nrf2, Ho-1. The data are shown as the mean ± SD; *$p < 0.05$, * *$p < 0.01$ vs control.

microscope (Olympus, Japan).

2.4. Cell culture and treatment

The rat H9c2 cardiomyocytes of the subculture adherent cell line used in the experiment was purchased from Boster Biological Technology co., Ltd, Wuhan, China. Cell culture were cultured in a 5–15% complete culture medium and placed in 25 cm^2 or 75 cm^2 culture bottles under the conditions of 37 ℃ and 5% CO_2. The complete culture medium was synthesized from DMEM high glucose medium (Boster, China), selected standard fetal bovine serum and penicillin-streptomycin double antibiotics (Solarbio, China). NaF and $NaAsO_2$ powders were diluted with 5% complete medium for the required stock solution.

In this experiment, to explore the interaction between arsenic and fluoride, the cells were divided into 9 groups based on the factorial design: Control group (C group, 0 μM $NaAsO_2$, 0 mg/L NaF), high arsenic and high fluoride group ($As_{25}F_{35}$ group, 25 μM $NaAsO_2$, 35 mg/L NaF), high arsenic and low fluoride group ($As_{25}F_{10}$ group, 25 μM $NaAsO_2$, 10 mg/L NaF), low arsenic and high fluoride group ($As_{10}F_{35}$ group, 10 μM $NaAsO_2$, 35 mg/L NaF), low arsenic and low fluoride group ($As_{10}F_{10}$ group, 10 μM $NaAsO_2$, 10 mg/L NaF), high fluoride group (F_{35} group, 35 mg/L NaF), low fluoride group (F_{10} group, 10 mg/L NaF), high arsenic group (As_{25} group, 25 μM $NaAsO_2$), low arsenic group (As_{10} group, 10 μM $NaAsO_2$). H9c2 cardiomyocytes were incubated with multiple concentrations of NaF and $NaAsO_2$ for 24 h. The exposure doses were based on our previous research and the exploration and adjustment in this experiment (Yan et al., 2017). Each cell experiment data represented the averages of 3 independent experiments.

2.5. Assessment of reactive oxygen species (ROS)

The ROS expression level was assessed by the cell ROS assay kit (Beyotime Institute of Biotechnology, China). The H9c2 cardiomyocytes, were digested, harvested and washed with PBS for 3 times (1500 r/min, 5 min each). After washing, PBS was discarded, and 1 ml of ROS reagent was added to each centrifuge tube, which was placed in an oven at 37 ℃ and incubated for 30 min. During this period, the

centrifuge tube is shaken every 5 min to ensure full reaction. After incubation in the dark, the supernatant was centrifuged and washed for 3 times. Finally, the expression of ROS in the cells was detected by flow cytometer (Becton, Dickinson and Company, USA).

2.6. Observation of transmission electron microscopy (TEM)

The apex of heart tissue was cut into small pieces less than 1 mm^3, fixed in 2.5% glutaraldehyde, and stored at 4 ℃ for 2 h. The apical tissue was dehydrated and sealed in epoxy resin. The tissue was cut and observed under transmission electron microscope. When H9c2 cells in 6-well plates grew to more than 10^6, they were digested with trypsin and transferred to EP tubes. PBS was added and centrifuged at a 1000 r/min for 5 min to remove the supernatant. Then, 2% pentylenediol was added and sample was let stand at 4 ℃ for 30 min. The cells were transferred into a 5 ml EP tube, fixed for 1.5 h, sectioned and observed under transmission electron microscope.

2.7. Quantitative RT-PCR analysis

Total RNA was extracted from myocardial tissue and cardiomyocytes using Trizol reagent (Takara, China). Concentrations of RNA were determined by measuring the absorbance at 260 nm using a UV spectrophotometer (BioTek, USA). RNA was reversely transcribed into cDNA using the TransScript One-Step gDNA Removal kit. Q-PCR was performed in a 20 μl reaction mixture prepared with SYBR GREEN PCR Master Mix (Takara, China) containing an appropriately diluted cDNA solution and 0.2 mM of each primer at 95 °C for 30 s, followed by 40 cycles of denaturation at 95 °C for 5 s, annealing at 60 °C for 30 s, and extension at 72 °C for 30 s. The transcript levels of Nrf2, Ho-1, Beclin1, LC3, p62 were detected by Quant-Studio 7 Flex Real-Time PCR System (Line Gene 9660, Bori, China). The qRT-PCR was performed in triplicate and repeated in at least three separate experiments. Data analysis was performed using $2^{-\Delta\Delta CT}$ method and β-actin was used as an internal control. The primers were listed in Table 1.

2.8. Total protein extraction and Western blotting analysis

After treatment, the tissue and cells were homogenized in RIPA lysis buffer (lysate: PMSF reagent: broad-spectrum phosphatase inhibitor = 100:1:1 in volume). The samples were centrifuged at 12000 r/min, 4 °C for 10 min. The supernatant was extracted as the total protein, and the concentration was determined by the Protein Quantitative Reagent Kit-BCA Method (Boster, China). Each 30 μg of protein sample was loaded on sodium dodecyl sulfate-polyacrylamide gels (10% separating gel, 5% concentrated gel) for electrophoresis at 80 V for 120 min. Following electrophoretic separation, the proteins were transferred to a nitrocellulose membrane, where they were blocked using 5% skimmed milk powder for 1 h, and then incubated with antibodies specific to Beclin1 (autophagy-related gene Atg6) (1:1000) (No. 3495, Cell Signaling Technology, USA), p62 (ubiquitin-binding protein p62) (1:1000) (No. 23214, Cell Signaling Technology, USA), LC3 (microtubule-associated proteins light chain 3) (1:1000) (No. 4108, Cell Signaling Technology, USA) and β-actin (1:4000) (No. ab8227, Abcam, UK) overnight at 4 °C. After washing three times with Tris-buffered saline with Tween 20, the membrane was incubated with HRP-conjugated secondary antibodies (1:4000) for 60 min at room temperature. After another three washes, the immunoreactive bands were detected by an ECL luminescence reagent (Boster, China) and observed using an electrophoresis gel imaging and analysis system (G:Box Chemi XX9; Syngene, UK).

Table 1
Primer sequences with their corresponding PCR product size and gene accession number.

Gene	Primer sequence (5–3′)	Primer length (bp)	Accession no
Nrf2-F	TTGGCAGAGACATTCCCATTTGTA	24	NM_031789.2
Nrf2-R	GAGCTATCGAGTGACTGAGCCTGA	24	
Ho-1-F	AGGTGCACATCCGTGCAGAG	21	NM_012580.2
Ho-1-R	CTTCCAGGGCCGTATAGATATGGTA	25	
Lc3-F	AGCTCTGAAGGCAACAGCAACA	22	NM_022867.2
Lc3-R	GCTCCATGCAGGTAGCAGGAA	21	
p62-F	AAGCTGCCCTGTACCCACATC	21	NM_175843.4
p62-R	ACCCATGGACAGCATCTGAGAG	22	
Beclin1-F	GAAACTGGACACGAGCTTCAAGA	23	NM_001034117.1
Beclin1-R	ACCATCCTGGCGAGTTTCAATA	22	
β-Actin-F	GGAGATTACTGCCCTGGCTCCTA	23	NM_031144.2
β-Actin-R	GACTCATCGTACTCCTGCTTGCTG	24	

2.9. Immunofluorescence analysis

Cell slides were prepared in 24-well plates and treated with arsenic and/or fluoride. The medium was discarded and washed in PBS for 3 times. Then, 1 ml of 4% paraformaldehyde solution was added into each well and fixed for 15 min. Add PBS and wash three times, 5 min each time. The cells were permeated with 0.5% T-X100 reagent for 15 min, and then washed with PBS for 3 times. After that, 500 μl of 10% donkey serum (Absin Bioscience, China) was added and sealed at room temperature for 30 min. Then, it was directly dropped into the antibodies of p62 (1:800) (No. 23214, Cell Signaling Technology, USA) and LC3 (1:100) (No. 4108, Cell Signaling Technology, USA) diluted with 2% BSA and incubated overnight at 4 ℃. Subsequently, immunofluorescence secondary antibodies (FITC and CY3) (Absin Bioscience, China) were added for reaction and incubated for 1 h in dark light. Wash PBS for 3 times, add DAPI dye solution to dye the core for 5 min. Then seal it with glass slides and anti-quench agent, and store it in a low temperature and dark place. Olympus fluorescence microscope (Olympus, Japan) was used for observation, and ImageJ software was used to analyze the differences in the average fluorescence intensity of proteins among groups.

2.10. Statistical analysis

The experimental data of arsenic-fluoride exposure were consistent with the 2 × 3 and 2 × 2 factorial design data, and the interaction between arsenic and fluoride was analyzed by the general linear model single-variable statistical method by SPSS 22.0 software. The test standard was $p < 0.05$. If there is no interaction, the main effects of arsenic and fluoride are further analyzed. If there is interaction, the interaction is determined as synergistic or antagonistic by adding and multiplying.

In addition, SPSS 22.0 software was used to conduct pairwise comparison among groups through one-way analysis of variance. If the data conforms to a normal distribution, the LSD method is used, otherwise the Dunnett's T3 method is used. The test standard was $p < 0.05$. GraphPad Prism 7.0 software was used for plotting.

3. Results

3.1. Arsenic and fluoride exposure induced myocardial injury accompanied by oxidative stress in myocardial tissue

To better mimic actual environment of combined exposure to arsenic and fluoride, we have established the 2 × 2 factorial design (two factor and two level) animal model that was initially exposed to arsenic and/or fluoride in the early life (in utero and childhood), indicating the interaction between arsenic and fluoride (Fig. 1A). Compared to control

group, the organ coefficient was reduced in all treated groups, and the decrease was statistically significant in F and F+As group (Fig. 1B). LDH, a hallmark enzyme of myocardial injury, its activity steadily increased after exposure to arsenic and fluoride (Fig. 1C). Na^+/K^+ ATPase is an important membrane protease involved in energy release, metabolite transportation and other important life activities (Marck et al., 2021). Arsenic and fluoride remarkably decreased the activity of ATPase, suggesting that the toxicity may destroy the permeability of the myocardial membrane (Fig. 1D).

Oxidative stress has been considered as a major factor leading to structural and functional abnormalities of the cardiovascular system (Yan et al., 2015). In myocardial tissue, the influences of arsenic and fluoride on oxidative stress were evaluated in Fig. 1E. The antioxidant enzyme activity of SOD and GSH-Px were decreased in all exposure groups. Compared to control group, the MDA significantly increased in As and F+As group (Fig. 1D). Additionally, the expression levels of antioxidant enzymes downstream genes Nrf2(nuclear factor erythroid 2-related factor-2) and Ho-1(heme oxygenase 1) were also reduced to varying degrees in all exposure groups.

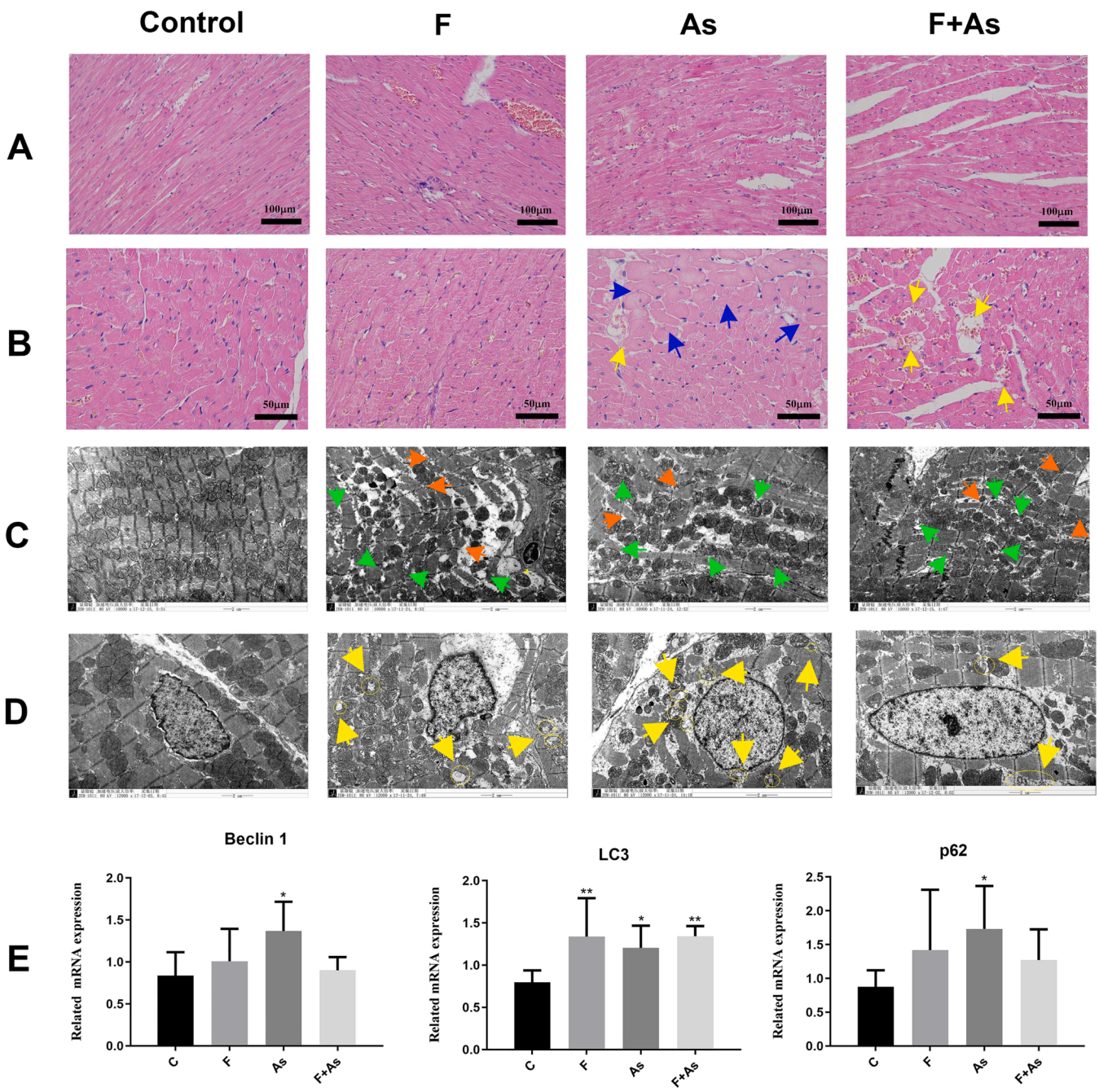

Fig. 2. Arsenic and fluoride exposure induced pathological changes and autophagy in myocardial tissue. (A-B) Histopathological changes in myocardial tissue (Bar=100 μm&50 μm). The yellow arrows represent inflammatory cell infiltration, and the blue arrows represent Swollen cells. (C) Ultrastructure of nucleus and mitochondria in myocardial tissue (Bar=2 μm). The orange arrows represent mitochondria, the green arrows represent myocardial fibers. (D) Distribution of autophagosomes around nuclei in myocardial tissue (Bar=2 μm). The yellow arrows represent autophagosomes. (E) Expression levels of autophagy-related genes Beclin1, LC3 and p62. The data are shown as the mean ± SD; *$p < 0.05$, * *$p < 0.01$ vs control.

3.2. Arsenic and fluoride exposure induced pathological changes and autophagy in myocardial tissue

Furthermore, the pathological changes of myocardial tissue were observed through optical microscopy and TEM. As shown in Fig. 2A-B, arsenic and fluoride led to irregular arrangement of the myocardial fibers, inflammatory cell infiltration, and cell swelling, and these changes were more severe in As and F+As group. Moreover, mitochondria, myocardial fibers of the myocardial ultrastructure were evaluated used TEM. In response to arsenic and fluoride, there were disordered and vacuolated mitochondria, irregularly arranged and broken myocardial fibers (Fig. 2C).

Transmission electron microscopy is the gold standard for the detection of the number and structure of autophagosomes (Klionsky et al., 2007). In the observed process of myocardium ultrastructure, we found the distribution of autophagosomes in toxin-exposed groups, including the autophagosome that surrounds the structure of multivesicular body and mitochondria and the advanced stage autophagosomes (Fig. 2D). Beclin1, LC3 and p62 are autophagic marker genes and play an important role in each stage of autophagy flow (Klionsky et al., 2007). The results indicated that mRNA levels of these genes were enhanced in all toxin-exposed groups (Fig. 2E). Compared to control group, the Beclin1 and p62 level were significantly enhanced in As group. Compared to control group, the LC3 level significantly increased in all exposure group.

3.3. Arsenic and fluoride exposure induced ultrastructural changes accompanied by oxidative stress in H9c2 cardiomyocytes

Subsequently, we explored whether the changes observed in above in vivo experiment occurred in H9c2 cells. As is shown in Fig. 3A, to elucidate the interaction between arsenic and fluoride in the process of myocardial injury, the H9c2 cells were divided into 9 groups based on the 2×3 factorial design (two factor and three level).

As shown in Fig. 3B, 24 h was selected as optimal exposure time, and 10 μM and 25 μM were selected as two factors in $NaAsO_2$ level, and 10 mg/L and 35 mg/L become two factors in NaF level. Furthermore, the survival rates of cardiomyocytes in the $As_{25}F_{35}$ group and $As_{25}F_{10}$ group were 66.2% and 75.4%, respectively, significantly lower than those of the control group. As shown in Fig. 3 C, the ROS content significantly increased in F_{35} group and As_{25} mediated single and combined groups, among which the ROS was the highest in the $As_{25}F_{35}$ group. Interestingly, intracellular ROS levels were dramatically lower in the As_{10} mediated single and combined groups. These data forcefully suggest that the two factors (As_{10} and As_{25}) at arsenic level were obviously cause opposite effects on ROS level.

Consistent with tissue results, significant changes in mitochondrial structure were observed in the exposure groups. As shown in Fig. 3D, the mitochondrial cristae were clear in the control group. After arsenic and fluoride exposure separately, the mitochondria were vacuolized to different degrees, and the F_{35} group showed mitophagy. In the four combined groups, only the mitochondria in the $As_{25}F_{35}$ group were partially vacuolated and mitophagy was also observed, while the other combined groups had intact mitochondrial structure without obvious vacuolation.

3.4. Arsenic and fluoride exposure increased autophagosomes in H9c2 cardiomyocytes

We further determined the mechanism of autophagy in arsenic and fluoride induced myocardial damage. Firstly, the changes in the number and ultrastructure of autophagosomes can accurately reflect the autophagy process (Fig. 4A). There are a greater number of autophagosomes in As_{25} and As_{10} group than F_{10} and F_{35} group, and the number of autophagosomes in the $As_{25}F_{10}$ and $As_{25}F_{25}$ group were more than $As_{10}F_{10}$ and $As_{10}F_{25}$ group. Additionally, it is known that the mature autophagosomes and lysosomes fuse to form a monolayer membrane structure of autophagosomes (Klionsky et al., 2007). We also observed the monolayer autophagic lysosome (containing mitochondria and other electron-dense cell components) in $As_{25}F_{10}$, $As_{25}F_{25}$ and As_{25} group, and autophagy precursors were found in $As_{25}F_{10}$, $As_{10}F_{10}$ and As_{10} group.

3.5. Arsenic and fluoride exposure affected autophagy related factors expression in H9c2 cardiomyocytes

To confirm the results observed by TEM, the qualitative and quantitative experiments were employed to detect the autophagic genes expression and distribution of targeted genes (Fig. 4A-D). The results of mRNA and protein level showed that the toxic exposure significantly increased Beclin1 expression in the $As_{25}F_{35}$ group and the As_{25} group. Conversely, it remarkably decreased in the $As_{10}F_{10}$ group and the F_{35} group. Moreover, the levels of LC3, a key protein responsible for autophagosomes accumulation, were dramatically increased in the As_{25} mediated single and combined groups. These LC3 results are consistent with the distribution of autophagosomes observed by TEM, indicating As_{25} may play a more significant role in autophagosome formation. P62, as another important marker of autophagy, also plays a crucial role in the formation and degradation of autophagosomes. The change of p62 gene and protein expression level was basically consistent, and except the F_{35} group, F_{10} group and $As_{10}F_{10}$ group, it was significantly increased in the other groups.

In addition, immunofluorescence was further used to verify the distribution and expression levels of autophagy-related proteins LC3 and p62 in H9c2 cell. After the formation of autophagosomes, LC3-I was converted to LC3-II and attached to the autophagosome membrane, which showed green fluorescent spots under a fluorescent microscope, and p62 showed red fluorescent spots. As shown in Fig. 4C-D, fluorescence autophagosomes were obviously found in As_{25} mediated single and combined groups, indicating that under the condition of high-arsenic exposure, the formation or degradation inhibition of autophagosomes were more significant, leading to a large number of autophagosomes in the cell. These results of fluorescence autophagosomes are in consonance with the distribution of autophagosomes observed by TEM. The expression of LC3 protein fluorescence signal intensity was only significantly increased in the $As_{25}F_{35}$ group. Moreover, the expression levels of p62 protein fluorescence signal intensity were significantly enhanced in As_{25} mediated single and combined groups, which was consistent with the previous results.

Overall, in H9c2 cell, these above findings suggest that Beclin1, LC3, and p62 were stimulated in all exposure groups except F_{35} and F_{10} group, which promoted the formation of autophagosome and inhibited the degradation of autophagosome. In addition, compared with As_{25} level groups ($As_{25}F_{35}$, $As_{25}F_{10}$, As_{25}), the As_{10} level groups ($As_{10}F_{35}$, $As_{10}F_{10}$, As_{10}) had a lower level of LC3 and p62.Fig. 1.

(A) The mRNA expression levels of autophagy-related genes Beclin1, LC3 and p62. (B) Expression levels of autophagy-related proteins. (C-D) Immunofluorescence results and semi-quantitative analysis results of autophagy-related proteins. Red: p62-positive puncta; green: LC3-positive puncta; blue: DAPI staining (Bar = 20 μm). The data are shown as the mean ± SD (n = 3); $*p < 0.05$, $**p < 0.01$and $***p < 0.001$ vs control.

3.6. Analysis of the interaction between arsenic and fluoride in each index

To explore whether there is an interaction between arsenic and fluoride in the process of cell damage and autophagy induction, this study used factorial analysis to analyze the results of multiple indicators (Table 2). For myocardial cells, the four indicators ROS, Beclin1 protein level, p62 mRNA and protein level results showed that arsenic and fluoride exposure may produce the interaction. In addition, all LC3 indicators showed the arsenic dominant effects. Only Beclin1 mRNA level showed the fluoride dominant effects. For myocardial tissue, there no

A

2×3 Factorial design		Sodium fluoride (NaF)		
		0mg/L	10mg/L	35mg/L
Sodium arsenite ($NaAsO_2$)	0 μM	Control	Low fluoride	High fluoride
	10 μM	Low arsenic	Low arsenic and low fluoride	Low arsenic and high fluoride
	25 μM	High arsenic	High arsenic and low fluoride	High arsenic and high fluoride

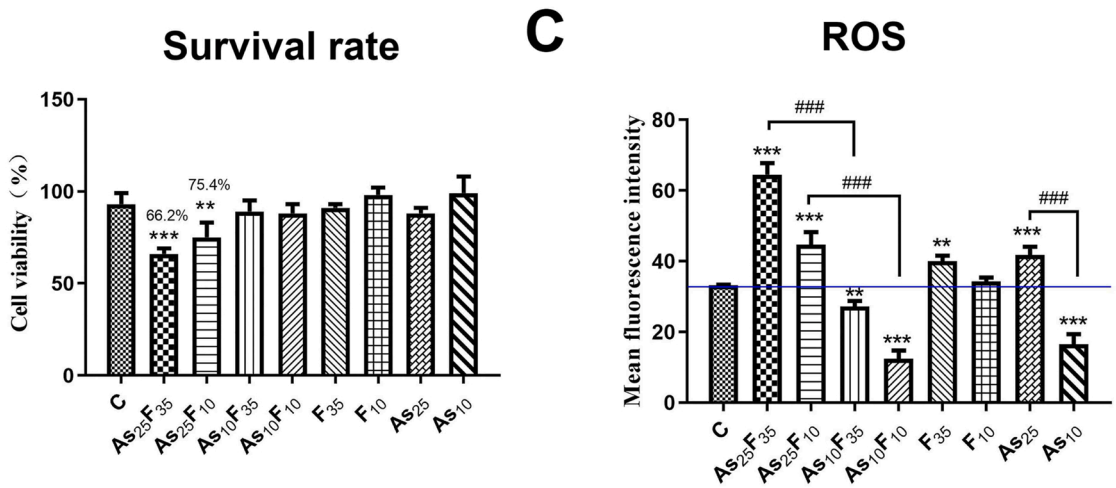

D

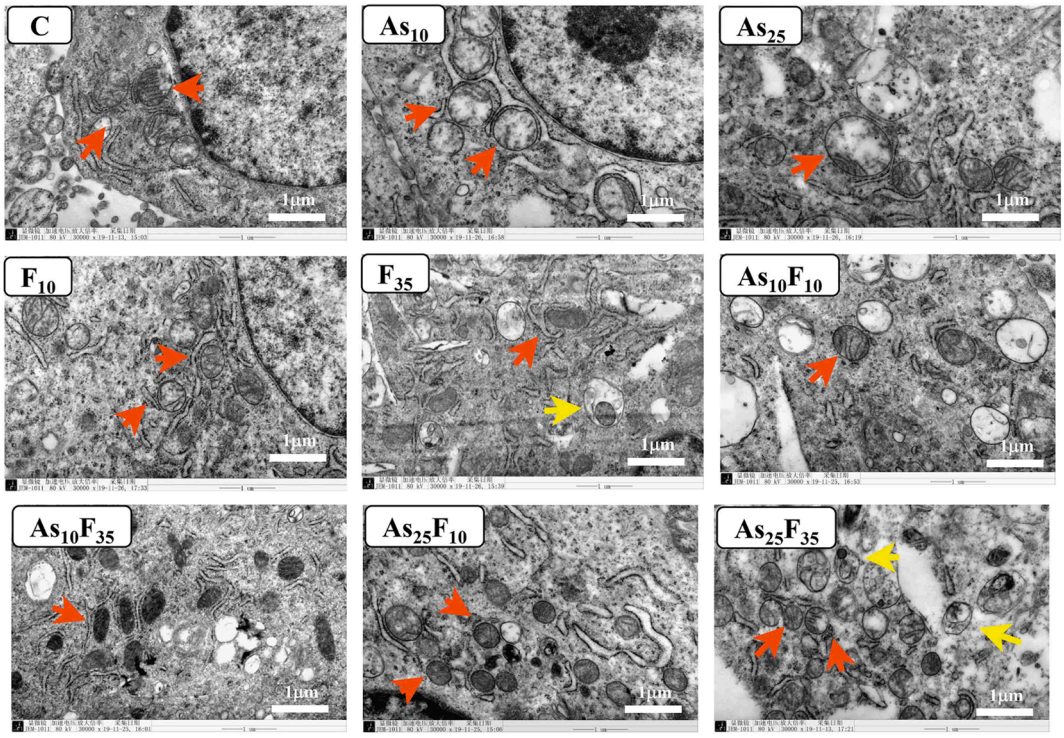

Fig. 3. Arsenic and fluoride exposure induced myocardial injury in H9c2 cardiomyocytes. (A) The H9c2 cardiomyocytes were grouped into 9 groups based on the 2×3 factorial design. H9c2 cardiomyocytes were exposed to 10 μM $NaAsO_2$, 25 μM $NaAsO_2$, 10 mg/L NaF, 35 mg/L NaF for 24 h. (B) Survival rate of each group after 24 h. (C) Intracellular ROS determination by flow cytometry. (D) Mitochondrial ultrastructure of H9c2 cardiomyocytes (Bar = 1 μm). The orange arrows represent mitochondria, and the yellow arrows represent mitochondrial autophagy. The data are shown as the mean ± SD (n = 3); $^{**}p < 0.01$ and $^{***}p < 0.001$ vs control.

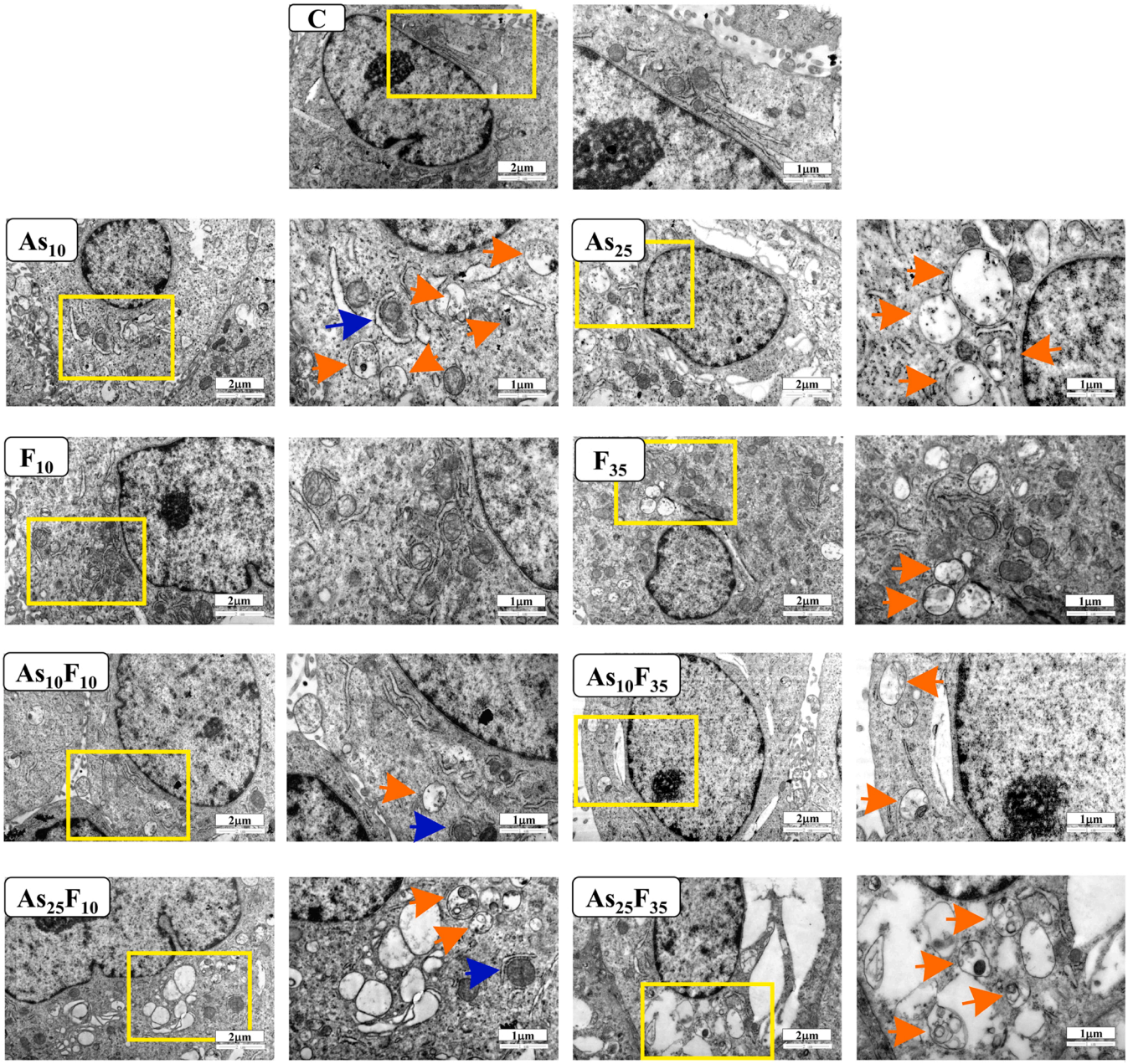

Fig. 4. Arsenic and fluoride exposure changes ultrastructure of autophagosome (Bar=1 μm&2 μm). The magnification of the left picture is 15,000 times, the right picture is 30,000 times, and the right picture is the part in the yellow box in the left picture. The orange arrows represent the autophagosomes, and the blue arrows represent the autophagy precursors.

interaction between arsenic and fluoride in all indexes. LDH and Ho-1 showed the arsenic and fluoride dominant effects. Na^+/K^+ ATPase and MDA showed the arsenic dominant effects. Beclin1 and LC3 mRNA level showed the fluoride dominant effects.

4. Discussion

Arsenic and fluoride are the most widespread and harmful co-existing pollutants in aquifers around the world (Chouhan and Flora, 2010). In this study, the principle of factorial design was used to conduct factorial trials in rats and cells, which was supported and asserted as an efficient means of assessing two factor (arsenic and fluoride) interventions simultaneously (McAlister et al., 2003). The rat and cell models are the factorial 2 × 3 and 2 × 2 design, and the independent variables are multi-level arsenic and fluoride exposure, furthermore, the various indicators on myocardial injury, oxidative stress and autophagy were measured to specifically explore these pollutants interaction. Using the animal model exposed to arsenic and fluoride, we found that these exposures led to aberrant changes of heart organ coefficient and myocardial enzyme. These results are consistent with reported studies in which high-dose of arsenic and fluoride induced the accumulation of myocardial enzyme (Panneerselvam et al., 2015; Sun et al., 2021). More importantly, our previous research has shown that co-exposure to arsenic and fluoride also caused adverse cardiac functions of blood pressure, echocardiogram, and electrocardiogram (Yan et al., 2021). Therefore, these above studies suggest that the adverse cardiovascular damage has been considered as one of targeting effect for combined toxicity of arsenic and fluoride.

Pathology changes, the typical biomarkers of organ-toxicity, were used to assess the degree of cardiovascular damage as a result of the

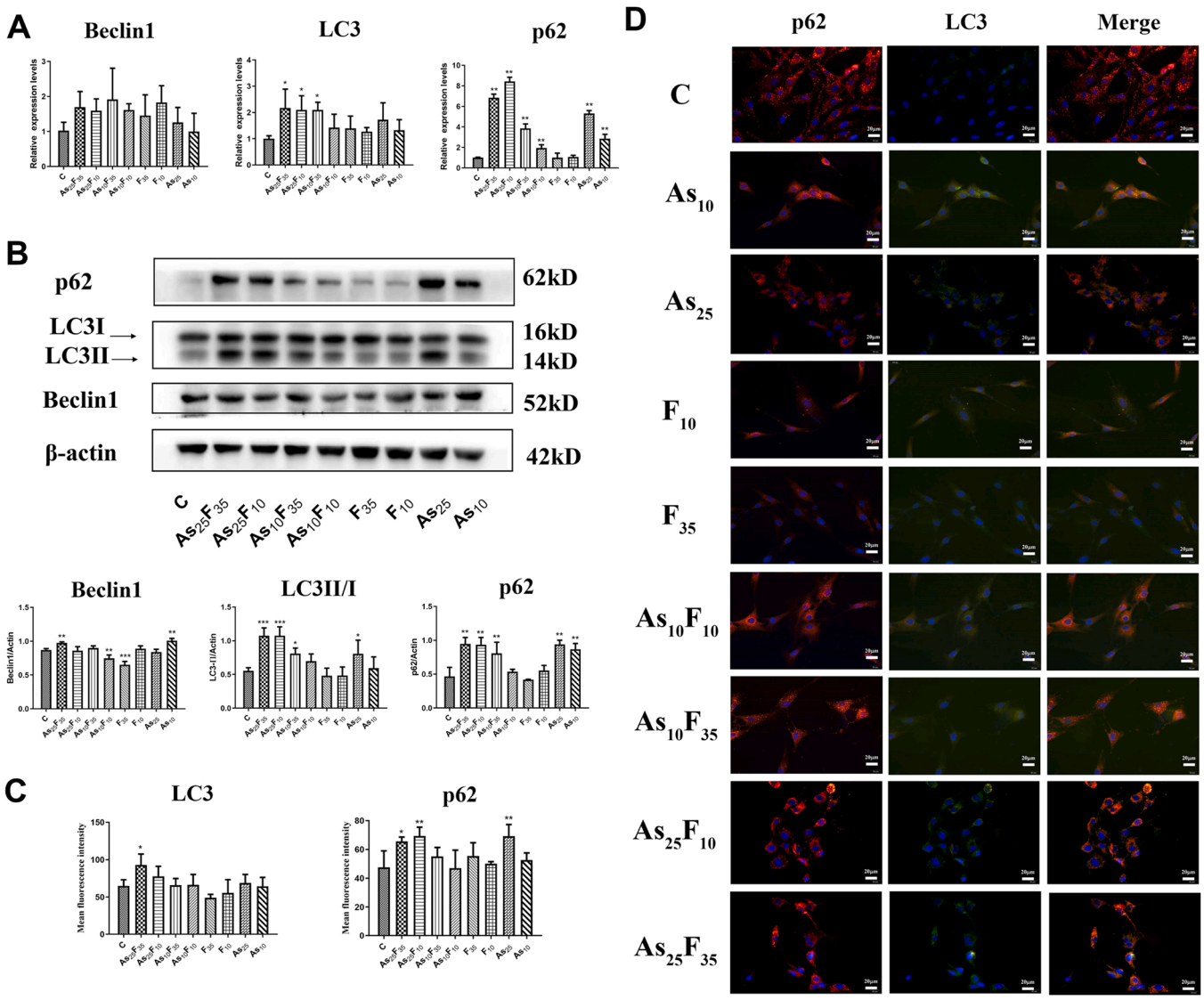

Fig. 5. Arsenic and fluoride exposure induced autophagy indexes alteration in H9c2 cardiomyocytes.

Table 2
Arsenic and fluoride interaction analysis of each indicator in cell and tissue.

	Indicators	The main effect of As		The main effect of F		As*F interaction	
		F value	P value	F value	P value	F value	P value
Cell	ROS	424.535	< 0.001	101.874	< 0.001	12.676	< 0.001 * *
	Beclin1 (PCR)	0.075	0.928	4.212	0.032##	0.51	0.729
	Beclin1 (WB)	13.354	< 0.001	8.834	0.002	32.704	< 0.001 * *
	p62 (PCR)	582.905	< 0.001	7.426	0.004	22.367	< 0.001 * *
	p62 (WB)	51.819	< 0.001	1.700	0.211	4.991	0.007 * *
	p62 (IF)	17.528	< 0.001##	0.437	0.652	1.047	0.411
	LC3 (PCR)	6.129	0.009##	2.97	0.077	0.401	0.806
	LC3 (WB)	31.883	< 0.001##	2.783	0.088	1.991	0.139
	LC3 (IF)	8.318	0.003##	0.173	0.843	2.029	0.133
Tissue	LDH	5.513	0.016##	11.524	0.004##	0.468	0.504
	Na^+/K^+ ATPase	7.207	0.017##	3.296	0.089	1.397	0.256
	SOD	3.297	0.084	4.353	0.050	2.071	0.166
	GSH-px	3.143	0.095	2.982	0.103	1.859	0.192
	MDA	12.758	0.003##	0.051	0.823	2.001	0.176
	Nrf2	1.559	0.230	7.088	0.017	3.732	0.071
	Ho-1	11.298	0.004##	4.906	0.042##	3.011	0.102
	Beclin1	2.334	0.146	5.455	0.033##	1.214	0.287
	LC3	2.713	0.119	7.419	0.015##	2.608	0.126
	p62	1.722	0.208	0.024	0.878	3.418	0.083

Note: * * represents $p < 0.05$, which means there is an interaction. ## represents the main effect.

combined exposure in the experiment (Stentiford et al., 2003). The results of hematoxylin and eosin staining showed that arsenic and fluoride induced irregular arrangement of the myocardial fibers, inflammatory cell infiltration, and cell swelling in myocardial tissue, moreover, these myocardial pathologic changes were also observed in H9c2 cells. The above findings are consistent with a previous study in which arsenic exposure leads to extensive necrosis, slight fiber swelling and interstitial edema, though acute gavage exposure way (Zhao et al., 2020). Similarly, H9c2 cardiomyocytes exposure to different concentrations of sodium fluoride impairs cellular morphology and induced apoptosis and morphological damage in our preceding study (Yan et al., 2017). It is of note that obvious vacuolation of mitochondria in myocardial cells showed the combined effect in the combined exposure groups, among which the $As_{25}F_{35}$ group was the most severe in our cell model. The similar combined effect has been evaluated in other organ histopathological damage caused by arsenic-fluoride combined exposure, such as liver, brain and kidney. Interestingly, compared to the individual exposure, these combined exposure to arsenic and fluoride did not result in significant exacerbation or reduction based on histopathological observations (Flora et al., 2012; Tian et al., 2020). Differences in the confounding factors (exposure time, dose and object) may account for this discrepancy about the combined effect of arsenic and fluoride.

Especially, mitochondria are typical target organelles for excessive free radical invasion and extremely vulnerable to oxidative stress (Yu et al., 2017). In our experiment, excessive ROS generation is accompanied by mitochondrial structural damage, verifying that arsenic and fluoride induced excessive oxidative stress damage in myocardial tissue. Moreover, in our study, arsenic and fluoride significantly changed mitochondrial structure and induced mitochondrial vacuolation, both in vivo and in vitro. Mitochondria are the main source of ROS production, and excessive ROS will also damage mitochondrial proteins and lipids, thus damaging the functional and structural properties of mitochondria (Wilson et al., 2019). It is imaginable that mitochondrial dysfunction is accompanied by the occurrence of excessive oxidative stress in the exposed groups. Undoubtedly, in current study, arsenic and fluoride remarkably decreased the antioxidant enzyme activity of SOD and GSH-PX, whereas increased accumulation of lipid peroxidation products in myocardial tissue. In order to response to excessive oxidative stress, Nrf2 protection mechanism is initiated along with the changes of its multiple downstream genes such as Nrf2 and Ho-1 (Dodson et al., 2015). Our results also showed that the reduction of Nrf2 and Ho-1 to varying degrees in all toxin-exposed groups. Unexpectedly, our cell results showed ROS content of H9c2 cells was significantly increased in As_{25} mediated single and combined groups, while decreased in As_{10} mediated single and combined groups, which was consistent with the previous study in human fibroblast cell lines and tumor cells (Lau et al., 2013; Snow et al., 2005). These data forcefully suggest that the two factors (As_{10} and As_{25}) at arsenic level were obviously cause opposite effects on ROS level, becoming the important breakthrough point to clarify the interaction of arsenic and fluoride in the later analysis.

Except the above a series of results, including ROS level, mitochondrial damage structure, we further discovered the extensive distribution of autophagosomes, implying that autophagy may become a potential target for the interaction mechanism of arsenic and fluoride. Autophagy is a dynamic process that involved the initiation, formation, maturation, and degradation of the autophagosome, which is rigorously controlled by a set of autophagy-related genes (Aki et al., 2013). In animal model, combined with accumulation of autophagosomes and the increase of Beclin1, LC3, p62, we indicated that the autophagosomes were unable to be further degraded accompanied by continuous generation and maturation of autophagosomes numerous under the arsenic and fluoride combined exposure. Additionally, in cell model, the toxics exposure significantly increased Beclin1 expression in the $As_{25}F_{35}$ group and the As_{25} group, meanwhile, the results of LC3, p62 level and autophagosomes also shown that the most significant increase in the As_{25} mediated groups. Specially, compared with As_{25} level groups ($As_{25}F_{35}$, $As_{25}F_{10}$, As_{25}), the As_{10} level groups ($As_{10}F_{35}$, $As_{10}F_{10}$, As_{10}) had a lower level of LC3 and p62. It is well known that there is a potential relationship between oxidative stress and autophagy, and they are important regulators between each other, to maintain or perturb the homeostasis in cells (Filomeni et al., 2015; Tai et al., 2017). In addition, previous studies have shown that arsenic-induced ROS stimulated autophagy by inhibiting mTOR pathway, inversely, appropriate autophagy carry out the important self-protection mechanism to efficaciously against the damage of excessive oxidative stress by arsenic exposure (Fang et al., 2021; Zhang et al., 2012). Therefore, in our study, we speculate the varying degrees of autophagy between As_{25} and As_{10} may become the important breakthrough point for explain the opposite effects of As_{25} and As_{10} on ROS level in our study. Significantly, early during the low-level arsenic exposure, oxidative stress level is not enhanced, and autophagy is impaired but tries to recover in response to the toxic environment of the organism (Zhong et al., 2021). Consistently, as the protective factor, autophagy against the ROS mediated low arsenic toxicity process in NCTC-1469 cells (Zhong et al., 2021). These data forcefully explain that the opposite effects on ROS level caused by two different doses (As_{10} and As_{25}) in our cell model, it is speculated that the proper occurrence of autophagy may reduce ROS cumulation at the low-arsenic level, while this effect was not observed at high arsenic level.

Based on the results of oxidative stress and autophagy in the animal and cell model experiments, whether clarifying the relationship between arsenic and fluoride, has become the crucially discussed part in this paper. In the rat myocardial damage model of 2×2 factorial design, there no interaction between arsenic and fluoride in all indexes although the main effects of arsenic or fluoride were confirmed in LDH, Na^+/K^+ ATPase, MDA, Ho-1 and LC3. Compared to in vivo experiments, in vitro studies are easier to steadily establish the factorial design toxicity models with multiple doses and time, so as to facilitate further explore the interactive toxic mechanism. Therefore, our 2×3 factorial design cell model was used to further elucidate the associative effect of arsenic and fluoride on oxidative stress. It is interesting to note in our cell model, we found the interaction in results of ROS content. Moreover, arsenic and fluoride showed a series of interactive effects on autophagy levels in our cell models. The results were consistent with the phenomenon that arsenic and fluoride induced autophagy through antagonistic mode in kidneys and testes of rat, and support the interaction on autophagy under arsenic and fluoride exposure (Liu et al., 2021; Tian et al., 2020). However, the antagonistic and synergistic effect on arsenic and fluoride still not fully understood. Several studies have shown that there is interaction between arsenic and fluoride on the oxidative stress, especially antagonism (Flora et al., 2009; Mittal et al., 2018; Mondal et al., 2019). Interestingly, a recent report showed synergy in assessing the combined effects of arsenic and fluoride on antioxidant enzymes in liver tissue, and scholars have proposed that identification of As and F binding domains (AsF, AsF_5) is essential to understand physiological relationship between As and F (Khan et al., 2022). Furthermore, under the multiple exposure times (30, 60, 90 days), there are different interactive effects (antagonistic or synergistic) in the toxic damage of liver and kidney exposed arsenic and fluoride (Huma, 2021). Based on above studies, the exposure dose and time have been important consideration to assess the relationship between arsenic and fluoride in future research.

5. Conclusions

The above results indicated that high arsenic (50 mg/L) and high fluoride (100 mg/L) induced myocardial injury, oxidative stress, autophagy during the cardiotoxicity process. In addition, we provide persuasive evidence that combined of arsenic-fluoride exposure possess the interactively influence on oxidative stress and autophagy, contributing to the cardiotoxicity. The findings provide novel interpretation into the phenomenon that co-contamination of arsenic and fluoride in groundwater, however, it's worth noting that more research are still

needed to further clarified the interactively toxic mechanism of these hazardous materials.

Funding

This work was supported by the National Natural Science Foundation of China (No. 82173644), the National Natural Science Foundation of China (No.82103961).

CRediT authorship contribution statement

Xiaolin Tian: Writing – original draft, Writing – review & editing, Conceptualization, Formal analysis, Methodology, Data curation. **Meng Wang**: Data curation, Formal analysis. **Xiaodong Ying**: Data curation, Formal analysis. **Meng Li:** Validation, Formal analysis.**Jing Feng:** Validation, Formal analysis. **Yannan Zhao**: Methodology. **Qian Zhao**: Funding acquisition. **Fengjie Tian:** Conceptualization. **Ben Li:** Resources.**Wenping Zhang:** Resources. **Yulan Qiu:** Supervision. **Xiaoyan Yan**: Writing – review & editing, Conceptualization, Supervision, Project administration, Funding acquisition.

Declaration of Competing Interest

The authors declare that they have no known competing financial interests or personal relationships that could have appeared to influence the work reported in this paper.

Data Availability

All data generated or analyzed during this study are included in this published article.

References

Aki, T., Funakoshi, T., Unuma, K., Uemura, K., 2013. Impairment of autophagy: from hereditary disorder to drug intoxication. Toxicology 311 (3), 205–215. https://doi.org/10.1016/j.tox.2013.07.001.

Alarcón-Herrera, M.T., Martin-Alarcon, D.A., Gutiérrez, M., et al., 2020. Co-occurrence, possible origin, and health-risk assessment of arsenic and fluoride in drinking water sources in Mexico: geographical data visualization. Sci. Total Environ. 698, 134168 https://doi.org/10.1016/j.scitotenv.2019.134168.

Armienta, M.A., Segovia, N., 2008. Arsenic and fluoride in the groundwater of Mexico. Environ. Geochem Health 30 (4), 345–353. https://doi.org/10.1007/s10653-008-9167-8.

Bundschuh, J., Farias, B., Martin, R., et al., 2004. Groundwater arsenic in the Chaco-Pampean Plain, Argentina: case study from Robles county, Santiago del Estero Province. Appl. Geochem. 19 (2), 231–243. https://doi.org/10.1016/j.apgeochem.2003.09.009.

Chakraborti, D., Rahman, M.M., Chatterjee, A., et al., 2016. Fate of over 480 million inhabitants living in arsenic and fluoride endemic Indian districts: magnitude, health, socio-economic effects and mitigation approaches. J. Trace Elem. Med Biol. 38, 33–45. https://doi.org/10.1016/j.jtemb.2016.05.001.

Che, Y., Wang, Z., Yuan, Y., et al., 2021. By restoring autophagic flux and improving mitochondrial function, corosolic acid protects against Dox-induced cardiotoxicity. Cell Biol. Toxicol. https://doi.org/10.1007/s10565-021-09619-8.

Chi, R.F., Li, L., Wang, A.L., et al., 2021. Enhanced oxidative stress mediates pathological autophagy and necroptosis in cardiac myocytes in pressure overload induced heart failure in rats. Clin. Exp. Pharm. Physiol. https://doi.org/10.1111/1440-1681.13583.

Chouhan, S., Flora, S.J., 2010. Arsenic and fluoride: two major ground water pollutants. Indian J. Exp. Biol. 48 (7), 666–678.

Daniels, L.J., Varma, U., Annandale, M., Chan, E., Mellor, K.M., Delbridge, L.M.D., 2019. Myocardial energy stress, autophagy induction, and cardiomyocyte functional responses. Antioxid. Redox Signal 31 (6), 472–486. https://doi.org/10.1089/ars.2018.7650.

Dodson, M., Redmann, M., Rajasekaran, N.S., Darley-Usmar, V., Zhang, J., 2015. KEAP1-NRF2 signalling and autophagy in protection against oxidative and reductive proteotoxicity. Biochem J. 469 (3), 347–355. https://doi.org/10.1042/bj20150568.

Fang, S., Wan, X., Zou, X., et al., 2021. Arsenic trioxide induces macrophage autophagy and atheroprotection by regulating ROS-dependent TFEB nuclear translocation and AKT/mTOR pathway. Cell Death Dis. 12 (1), 88. https://doi.org/10.1038/s41419-020-03357-1.

Filomeni, G., De Zio, D., Cecconi, F., 2015. Oxidative stress and autophagy: the clash between damage and metabolic needs. Cell Death Differ. 22 (3), 377–388. https://doi.org/10.1038/cdd.2014.150.

Flora, S.J., Mittal, M., Mishra, D., 2009. Co-exposure to arsenic and fluoride on oxidative stress, glutathione linked enzymes, biogenic amines and DNA damage in mouse brain. J. Neurol. Sci. 285 (1–2), 198–205. https://doi.org/10.1016/j.jns.2009.07.001.

Flora, S.J., Pachauri, V., Mittal, M., Kumar, D., 2011. Interactive effect of arsenic and fluoride on cardio-respiratory disorders in male rats: possible role of reactive oxygen species. Biometals: Int. J. Role Met. Ions Biol. Biochem. Med. 24 (4), 615–628. https://doi.org/10.1007/s10534-011-9412-y.

Flora, S.J., Mittal, M., Pachauri, V., Dwivedi, N., 2012. A possible mechanism for combined arsenic and fluoride induced cellular and DNA damage in mice. Metallomics 4 (1), 78–90. https://doi.org/10.1039/c1mt00118c.

González-Horta, C., Ballinas-Casarrubias, L., Sánchez-Ramírez, B., et al., 2015. A concurrent exposure to arsenic and fluoride from drinking water in Chihuahua, Mexico. Int J. Environ. Res Public Health 12 (5), 4587–4601. https://doi.org/10.3390/ijerph120504587.

Gu, X., Han, D., Chen, W., et al., 2016. SIRT1-mediated FoxOs pathways protect against apoptosis by promoting autophagy in osteoblast-like MC3T3-E1 cells exposed to sodium fluoride. Oncotarget 7 (40), 65218–65230. https://doi.org/10.18632/oncotarget.11573.

Huang, Y.K., Tseng, C.H., Huang, Y.L., Yang, M.H., Chen, C.J., Hsueh, Y.M., 2007. Arsenic methylation capability and hypertension risk in subjects living in arseniasis-hyperendemic areas in southwestern Taiwan. Toxicol. Appl. Pharmacol. 218 (2), 135–142. https://doi.org/10.1016/j.taap.2006.10.022.

Huma, Verma Y., Rana S Liver and kidney function in rats co-treated with fluoride and arsenic for different time intervals. In, 2021.

Khan, H., Verma, Y., Rana, S., 2022. Duration of exposure modulates combined effects of arsenic and fluoride on oxidative stress in the liver of rat. J. Environ. Biol. 43, 514–519. https://doi.org/10.22438/jeb/43/4/MRN-2083.

Klionsky, D.J., Cuervo, A.M., Seglen, P.O., 2007. Methods for monitoring autophagy from yeast to human. Autophagy 3 (3), 181–206. https://doi.org/10.4161/auto.3678.

Kumar, M., Goswami, R., Patel, A.K., Srivastava, M., Das, N., 2020. Scenario, perspectives and mechanism of arsenic and fluoride Co-occurrence in the groundwater: a review. Chemosphere 249, 126126. https://doi.org/10.1016/j.chemosphere.2020.126126.

Lau, A., Zheng, Y., Tao, S., et al., 2013. Arsenic inhibits autophagic flux, activating the Nrf2-Keap1 pathway in a p62-dependent manner. Mol. Cell Biol. 33 (12), 2436–2446. https://doi.org/10.1128/mcb.01748-12.

Li, M., Zhao, Y., Tian, X., et al., 2021. Fluoride exposure and blood pressure: a systematic review and meta-analysis. Biol. Trace Elem. Res. 199 (3), 925–934. https://doi.org/10.1007/s12011-020-02232-6.

Liu, P., Li, R., Tian, X., et al., 2021. Co-exposure to fluoride and arsenic disrupts intestinal flora balance and induces testicular autophagy in offspring rats. Ecotoxicol. Environ. Saf. 222, 112506 https://doi.org/10.1016/j.ecoenv.2021.112506.

Ma, Y., Niu, R., Sun, Z., et al., 2012. Inflammatory responses induced by fluoride and arsenic at toxic concentration in rabbit aorta. Arch. Toxicol. 86 (6), 849–856. https://doi.org/10.1007/s00204-012-0803-9.

Ma, Y., Ma, Z., Yin, S., Yan, X., Wang, J., 2017. Arsenic and fluoride induce apoptosis, inflammation and oxidative stress in cultured human umbilical vein endothelial cells. Chemosphere 167, 454–461. https://doi.org/10.1016/j.chemosphere.2016.10.025.

Marck, P.V., Pessoa, M.T., Xu, Y., Kutz, L.C., Pierre, S.V., 2021. Cardiac oxidative signaling and physiological hypertrophy in the Na/K-ATPase α1s/sα2s/s mouse model of high affinity for cardiotonic steroids. Int. J. Mol. Sci. 22 (7), 3462. https://doi.org/10.3390/ijms22073462.

McAlister, F.A., Straus, S.E., Sackett, D.L., Altman, D.G., 2003. Analysis and reporting of factorial trials: a systematic review. Jama 289 (19), 2545–2553. https://doi.org/10.1001/jama.289.19.2545.

Mittal, M., Chatterjee, S., Flora, S.J.S., 2018. Combination therapy with vitamin C and DMSA for arsenic-fluoride co-exposure in rats. Metallomics 10 (9), 1291–1306. https://doi.org/10.1039/c8mt00192h.

Mondal, P., Chattopadhyay, A., 2020. Environmental exposure of arsenic and fluoride and their combined toxicity: a recent update. J. Appl. Toxicol. 40 (5), 552–566. https://doi.org/10.1002/jat.3931.

Mondal, P., Shaw, P., Bandyopadhyay, A., et al., 2019. Mixture effect of arsenic and fluoride at environmentally relevant concentrations in zebrafish (Danio rerio) liver: Expression pattern of Nrf2 and related xenobiotic metabolizing enzymes. Aquat. Toxicol. 213, 105219 https://doi.org/10.1016/j.aquatox.2019.06.002.

Moon, K., Guallar, E., Navas-Acien, A., 2012. Arsenic exposure and cardiovascular disease: an updated systematic review. Curr. Atheroscler. Rep. 14 (6), 542–555. https://doi.org/10.1007/s11883-012-0280-x.

Oyagbemi, A.A., Omobowale, T.O., Asenuga, E.R., et al., 2017. Sodium fluoride induces hypertension and cardiac complications through generation of reactive oxygen species and activation of nuclear factor kappa beta. Environ. Toxicol. 32 (4), 1089–1101. https://doi.org/10.1002/tox.22306.

Panneerselvam, L., Govindarajan, V., Ameeramja, J., Nair, H.R., Perumal, E., 2015. Single oral acute fluoride exposure causes changes in cardiac expression of oxidant and antioxidant enzymes, apoptotic and necrotic markers in male rats. Biochimie 119, 27–35. https://doi.org/10.1016/j.biochi.2015.10.002.

Rocha, R.A., Gimeno-Alcañiz, J.V., Martín-Ibañez, R., Canals, J.M., Vélez, D., Devesa, V., 2011. Arsenic and fluoride induce neural progenitor cell apoptosis. Toxicol. Lett. 203 (3), 237–244. https://doi.org/10.1016/j.toxlet.2011.03.023.

Rocha-Amador, D., Navarro, M.E., Carrizales, L., Morales, R., Calderón, J., 2007. Decreased intelligence in children and exposure to fluoride and arsenic in drinking water. Cad. Saude Publica 23 (Suppl 4), S579–S587. https://doi.org/10.1590/s0102-311×2007001600018.

Sárközi, K., Horváth, E., Vezér, T., Papp, A., Paulik, E., 2015. Behavioral and general effects of subacute oral arsenic exposure in rats with and without fluoride. Int J. Environ. Health Res 25 (4), 418–431. https://doi.org/10.1080/09603123.2014.958138.

Simeonova, P.P., Hulderman, T., Harki, D., Luster, M.I., 2003. Arsenic exposure accelerates atherogenesis in apolipoprotein E(-/-) mice. Environ. Health Perspect. 111 (14), 1744–1748. https://doi.org/10.1289/ehp.6332.

Sivasankar V., Darchen A., Omine K., Sakthivel R. (2016) Fluoride: A World Ubiquitous Compound, Its Chemistry, and Ways of Contamination. Surface Modified Carbons as Scavengers for Fluoride from Water.

Snow, E.T., Sykora, P., Durham, T.R., Klein, C.B., 2005. Arsenic, mode of action at biologically plausible low doses: what are the implications for low dose cancer risk. Toxicol. Appl. Pharmacol. 207 (2 Suppl), 557–564. https://doi.org/10.1016/j.taap.2005.01.048.

Srivastava, S., D'Souza, S.E., Sen, U., States, J.C., 2007. In utero arsenic exposure induces early onset of atherosclerosis in ApoE-/- mice. Reprod. Toxicol.) 23 (3), 449–456. https://doi.org/10.1016/j.reprotox.2007.01.005.

Stentiford, G.D., Longshaw, M., Lyons, B.P., Jones, G., Green, M., Feist, S.W., 2003. Histopathological biomarkers in estuarine fish species for the assessment of biological effects of contaminants. Mar. Environ. Res 55 (2), 137–159. https://doi.org/10.1016/s0141-1136(02)00212-x.

Sun, X., Wang, X., He, Q., et al., 2021. Investigation of the ameliorative effects of baicalin against arsenic trioxide-induced cardiac toxicity in mice. Int Immunopharmacol. 99, 108024 https://doi.org/10.1016/j.intimp.2021.108024.

Tai, H., Wang, Z., Gong, H., et al., 2017. Autophagy impairment with lysosomal and mitochondrial dysfunction is an important characteristic of oxidative stress-induced senescence. Autophagy 13 (1), 99–113. https://doi.org/10.1080/15548627.2016.1247143.

Tian, X., Feng, J., Dong, N., et al., 2019. Subchronic exposure to arsenite and fluoride from gestation to puberty induces oxidative stress and disrupts ultrastructure in the kidneys of rat offspring. Sci. Total Environ. 686, 1229–1237. https://doi.org/10.1016/j.scitotenv.2019.04.409.

Tian, X., Xie, J., Chen, X., et al., 2020. Deregulation of autophagy is involved in nephrotoxicity of arsenite and fluoride exposure during gestation to puberty in rat offspring. Arch. Toxicol. 94 (3), 749–760. https://doi.org/10.1007/s00204-019-02651-y.

Tsuji, J.S., Perez, V., Garry, M.R., Alexander, D.D., 2014. Association of low-level arsenic exposure in drinking water with cardiovascular disease: a systematic review and risk assessment. Toxicology 323, 78–94. https://doi.org/10.1016/j.tox.2014.06.008.

Wang, K., Klionsky, D.J., 2011. Mitochondria removal by autophagy. Autophagy 7 (3), 297–300. https://doi.org/10.4161/auto.7.3.14502.

Wang, S.X., Wang, Z.H., Cheng, X.T., et al., 2007a. Arsenic and fluoride exposure in drinking water: children's IQ and growth in Shanyin county, Shanxi province, China. Environ. Health Perspect. 115 (4), 643–647. https://doi.org/10.1289/ehp.9270.

Wang, Y.H., Wu, M.M., Hong, C.T., et al., 2007b. Effects of arsenic exposure and genetic polymorphisms of p53, glutathione S-transferase M1, T1, and P1 on the risk of carotid atherosclerosis in Taiwan. Atherosclerosis 192 (2), 305–312. https://doi.org/10.1016/j.atherosclerosis.2006.07.029.

Wilson, R.J., Drake, J.C., Cui, D., et al., 2019. Conditional MitoTimer reporter mice for assessment of mitochondrial structure, oxidative stress, and mitophagy. Mitochondrion 44, 20–26. https://doi.org/10.1016/j.mito.2017.12.008.

Yamashita, S.I., Kanki, T., 2017. How autophagy eats large mitochondria: autophagosome formation coupled with mitochondrial fragmentation. Autophagy 13 (5), 980–981. https://doi.org/10.1080/15548627.2017.1291113.

Yan, X., Yang, X., Hao, X., et al., 2015. Sodium fluoride induces apoptosis in H9c2 cardiomyocytes by altering mitochondrial membrane potential and intracellular ROS level. Biol. Trace Elem. Res. 166 (2), 210–215. https://doi.org/10.1007/s12011-015-0273-z.

Yan, X., Wang, L., Yang, X., et al., 2017. Fluoride induces apoptosis in H9c2 cardiomyocytes via the mitochondrial pathway. Chemosphere 182, 159–165. https://doi.org/10.1016/j.chemosphere.2017.05.002.

Yan, X., Chen, X., Tian, X., et al., 2021. Co-exposure to inorganic arsenic and fluoride prominently disrupts gut microbiota equilibrium and induces adverse cardiovascular effects in offspring rats. Sci. Total Environ. 767, 144924 https://doi.org/10.1016/j.scitotenv.2020.144924.

Yi, C., Tong, J.J., Yu, L., 2018. Mitochondria: the hub of energy deprivation-induced autophagy. Autophagy 14 (6), 1084–1085. https://doi.org/10.1080/15548627.2017.1382785.

Yu, L., Chen, Y., Tooze, S.A., 2017. Autophagy pathway: cellular and molecular mechanisms, 00-00 Autophagy. https://doi.org/10.1080/15548627.2017.1378838.

Zhang, T., Qi, Y., Liao, M., et al., 2012. Autophagy is a cell self-protective mechanism against arsenic-induced cell transformation. Toxicol. Sci. 130 (2), 298–308. https://doi.org/10.1093/toxsci/kfs240.

Zhao, Y., Jia, W.W., Ren, S., et al., 2021. Difluoromethylornithine attenuates isoproterenol-induced cardiac hypertrophy by regulating apoptosis, autophagy and the mitochondria-associated membranes pathway. Exp. Ther. Med 22 (2), 870. https://doi.org/10.3892/etm.2021.10302.

Zhao, Z., Li, J., Zheng, B., et al., 2020. Ameliorative effects and mechanism of crocetin in arsenic trioxide-induced cardiotoxicity in rats. Mol. Med Rep. 22 (6), 5271–5281. https://doi.org/10.3892/mmr.2020.11587.

Zhong, G., Wan, F., Ning, Z., et al., 2021. The protective role of autophagy against arsenic trioxide-induced cytotoxicity and ROS-dependent pyroptosis in NCTC-1469 cells. J. Inorg. Biochem 217, 111396. https://doi.org/10.1016/j.jinorgbio.2021.111396.

Zhuang, H., Ali, K., Ardu, S., Tredwin, C., Hu, B., 2016. Autophagy in dental tissues: a double-edged sword. Cell Death Dis. 7 (4), e2192 https://doi.org/10.1038/cddis.2016.103.